Journal of
Manufacturing and Materials Processing

MDPI

Article

A Novel Method to Assess Aluminium Alloy Machinability Using Shear Cracks in Chips Formed During Machining

Abdul Radim Asil [1,2], Nilam S. Barekar [2], Carla Barbatti [2,3] and Dmitry G. Eskin [1,*]

[1] Brunel Centre for Advanced Solidification Technology, Brunel University of London, Uxbridge UB8 3PH, UK; radim.asil2@brunel.ac.uk
[2] Constellium Technology Centre, Uxbridge UB8 3PH, UK; nilam.barekar@constellium.com (N.S.B.); carla.barbatti@constellium.com (C.B.)
[3] Constellium Technology Centre, Parc Economique Centr'Alp, CS 10027, 38341 Voreppe Cedex, France
* Correspondence: dmitry.eskin@brunel.ac.uk

Abstract

Demand for aluminium (Al) products has increased due to their low density, high strength-to-weight ratio, thermal and electrical conductivity, and corrosion resistance. Reliable machinability assessment is important for selecting suitable alloys for manufacturing applications. However, conventional methods based on chip counting and weighing may not adequately distinguish alloys with similar chemical compositions. This study proposes an alternative method for assessing aluminium alloy machinability by quantifying the Shear Crack Initiation Layer (SCIL) in machining chips. Aluminium alloys were machined using a lathe under consistent machining parameters, and chip cross-sections were examined to quantify shear crack features and investigate differences between inner and outer chip layers. Conventional chip counting and weighing produced similar machinability values for two chemically similar alloys and showed negligible differences between the inner and outer layers of each alloy. In contrast, SCIL-based assessment revealed clear machinability differences between the inner and outer layers within each alloy and between the two chemically similar alloys. These findings demonstrate the potential of SCIL quantification to provide a more sensitive assessment of aluminium alloy machinability than conventional chip counting and weighing methods.

Keywords: machinability; shear cracks; chip morphology; chip formation; chip breakability; scanning electron microscopy

Check for updates

Academic Editors: Ivana Dumanić Labetić and Marina Crnjac Žižić

Received: 26 October 2026
Revised: 6 November 2026
Accepted: 9 November 2026
Published: 11 November 2026

Copyright: © 2026 by the authors. Licensee MDPI, Basel, Switzerland. This article is an open access article distributed under the terms and conditions of the Creative Commons Attribution (CC BY) license.

1. Introduction

Aluminium has become an essential metal globally, widely used across numerous industries due to a distinctive combination of properties including low density, high strength-to-weight ratio, excellent thermal and electrical conductivity, and remarkable corrosion resistance, which is attributed to the formation of a protective oxide layer on an alloy's surface [1]. It is used in a wide range of products, including beverage cans, window and door frames, automobile and aircraft panels, and mobile or laptop casings, among others. Due to this versatility, techniques such as machining using an automated lathe for example, have been employed to create single piece parts from wrought products. Good machinability means low cycle times, reduced downtimes for cleaning and a good finished surface that is advantageous for further finishing such as painting, anodising or joining.

During the machining of Al alloys, chips are formed whilst creating a product [2]. Chip morphology has two typical extremes, referred to as continuous or discontinuous

morphologies, with every shade of gradation between the two types being observed [3]. Multiple parameters can be adjusted to control the morphology of chips formed such as, the rake angle, feed, depth of cut, cutting speed, tool geometry and workpiece material properties. There are two generic groups by which the methods for determining machinability can be assessed. One is predominantly focused on input parameters correlating with machinability, while the other is based on the aftermath of machining by assessing chip morphology/properties.

What can be gathered from literature is that there are a variety of existing methods that can determine the machinability of an alloy, a selection of which is summarised in this section. Standards which have been formulated to compare machinability of different workpiece materials have been developed. These include standards such as ISO 3685:1993 [4] and ISO 8688–1/2:1989 [5], which were produced to determine machinability using tool life, whereby the longer the tool life the better the machinability of the alloy. These standards are based on the tool-life equation, considering parameters such as the cutting speed, tool life, and constants based on the tool life index and machining index [6]. This method ultimately relies on the life of the tool to correlate machinability, which results in a tool being worn for the assessment to be made. This can be a wasteful method regarding the use of tools and samples as well as the associated financial cost.

Another widely used method to evaluate machinability is by assessing the cutting force required for an alloy to be machined. The cutting force can be estimated by using the power supplied to support the turning operation and the linear cutting speed, for example [7]. A lower cutting force for a chip to break off, where other parameters are kept the same, can be attributed to improved machinability. Spindle torque has also been correlated with cutting force, whereby the torque and the cutting force increased almost linearly with the feed rate [8]. Therefore, torque can also be used as an indicator in the assessment of alloy machinability where a higher torque can generally be attributed to a lower machinability.

Monitoring cutting temperature can be used to compare alloy machinability. Thermocouples embedded near the cutting edge can be used to measure cutting-zone temperature, where lower heat generation generally indicates better machinability [3]. Significant thermal gradients and rapid temperature changes near the tool edge using thermocouples were demonstrated [9–12]. However, it was argued that alloy inhomogeneity alone can introduce errors of at least 5% [13]. Thus, the errors can limit the method when comparing similar alloys where temperature differences may be small. Only modest differences were found in cutting voltages between AlSi7Mg0.3 and variants modified with Sr, Ca and Sb, suggesting that small compositional changes have limited influence on cutting temperature under comparable conditions [14]. Radiation can be measured from heated tool regions using a micro-photometer to determine temperature gradients [15]. This method, like thermocouples, may have insufficient sensitivity to distinguish closely related alloys. Resistance thermometry has also been used to assess machinability, with platinum resistance thermometers (PRTs) measuring temperature through changes in electrical resistance, where higher temperatures may indicate poorer machinability. A step further was taken to develop a custom-built system which integrates a PRT onto the cutting tool to provide highly localised measurements [16]. Despite this, uncertainty can arise from factors including radiation, lag and settling, thermal expansion, and thermal and mechanical shocks. Spectral radiation thermometry provides another approach to assessing machinability [17], although uncertainty is strongly influenced by emissivity, reflection, absorption, source size and field-of-view obstructions. Consequently, while temperature-based techniques are useful for general machining studies, their inherent measurement uncertainties and limited sensitivity make them less suitable for clearly distinguishing the machinability of alloys with only minor compositional differences.

Machinability can also be assessed by using the specific cutting energy and the undeformed thickness of the chips. An equation was developed where the less energy used for a given undeformed thickness, the better the machinability when comparing one alloy to another [18]. It is noted that the exponential increase in specific energy at a reduced undeformed chip thickness, can be attributed to the highly negative rake angles and increased ploughing and friction. This suggests other mechanisms can interfere and affect the machinability results rather than the specific cutting energy and/or the undeformed chip thickness. Therefore, it cannot be used alone in the assessment of alloy machinability.

Using surface-integrity methods provides additional ways to determine alloy machinability [19]. From the review, machinability may be evaluated through the condition of the machined surface and subsurface. This includes surface roughness, residual stress, microhardness, white-layer formation, and subsurface deformation within the surface-integrity category. Although surface-integrity-based methods provide a direct assessment of the functional quality of a machined component, they are inherently multi-parameter. Consequently, the review recommends evaluating machinability using multiple complementary indicators rather than a single surface-integrity metric. They state that there is currently no uniquely defined quantification of machinability.

There are two common methods of evaluating machinability [20]. One is achieved through making chip breaking curves by visual inspection to determine the point between acceptable and unacceptable chip breakage. The other is to create a chip chart to compare photos of the collected chips, from which the relevant cutting parameters can be selected to achieve adequate chip breaking. These methods are simple and inexpensive; however, they are reliant on the subjective view of the machining operator. While most machinists would agree on the machinability of an alloy with clearly distinctive chip formations, difficulties arise when chips appear similar in morphology and size. It is here where problems may arise, especially when dealing with an alloy and its variant (only differing slightly by composition).

The highlighted methods can be used as good indicators of machinability and would most likely be able to distinguish between significantly different alloys. However, in many cases industry develops an alloy and requires improvements typically made through chemical modification by adjusting the composition and/or the addition/removal of metallic additions. These methods may not be inherently sensitive enough to pick up on subtle changes in alloy chemistry and if they do, it could be acclaimed to a margin of error. In such cases, these methods may lack precision and can easily have overlapping results, where alloy machinability is said to be similar (be it subjectively or quantified) but the morphology of the chip from one alloy compared to a chip from another alloy is clearly different. Industry adopted a measure of machinability using a chip weight method assessing the swarf itself [20,21]; however, it has limitations, seen in the results section. There is a clear difference in the morphology of chips formed, but industrial quantification of machinability seems to show no significant difference. This difference is clearly significant based on chip morphology and by extension tool life, operator efficiency, the alloy's surface finish, among others. Additionally, the industrial method is laborious when assessing more than one alloy which requires several samples to be prepared. This can involve the manual counting of a few thousand chips, which takes both considerable time and puts some physical strain on the person counting due to the repetitive nature of the task over its duration.

As one can see, unlike most material properties, machinability generally has no accepted parameter used for its measurement [22]. This study aims to help work towards bridging this gap by introducing a new evaluation method to determine machinability using only one measured parameter from the collected swarf, with the assumption that all other machining inputs are kept the same when comparing said base alloy with a variant. This

study is relevant to both academia and industry, where a new simple method can provide improved data to inform decision making when designing/modifying alloys. This can give the competitive edge over other alloys in the market due to the improved assessment of machinability, where the data has a better match to the morphology/size of chips.

2. Materials and Methods

In this paper a new method is proposed to determine the machinability of a 6XXX series Al alloy (Constellium, Děčín. Czech Republic), which can in theory be applied to all Al alloys and potentially others such as steel, using swarf/chips collected from machining. The methods used begin with the machining of an Al alloy at certain depths of an alloy profile, from which the chips are collected and cleaned of any remaining cutting fluid. Several chips are collected and placed into a scanning electron microscope (SEM, Jeol IT200, Tokyo, Japan) for imaging of a key region used to then quantify the machinability of an alloy. The quantification of this key region and its correlation to machinability is the new proposed method. Further details of each step are provided in this section.

In this case, the chips originated from an aged extruded 33 mm in diameter AA6050 rod (Constellium, Děčín. Czech Republic) and an alloy variant with the additions 0.55 wt.% Ca and 0.27 wt.% Sr, which is known to have a better machinability using the weight method described in this section. A total of three shorter sample rods were taken from each extruded alloy for machinability trials. The composition of AA6050 is given in Table 1 [23]. A schematic in Figure 1 shows the locations from which the sample chips were taken as a result of machining. The machining parameters used were kept the same for both alloys. The aim of this study was not to investigate the effects of the parameters but rather to keep them constant with the variable being only the alloy composition. The turning operation was performed on an automated Chester CNC Slantbed Lathe CSL5530 machine (Burntwood, UK) using a CCGX 09 T3 04-AL H10/CCGX 3(2,5)1-AL H10 cutting insert (Sandvik Coromant, Sandviken, Sweden) at a speed of 141 m/min for a depth of cut of 2 mm and cutting length of 150 mm with cutting fluid. The feed rate was 0.3 mm/rev and the spindle power was 11 kW.

Table 1. Average nominal chemical composition (wt.%) of an AA6050 alloy [23].

Alloy	Al	Si	Fe	Mn	Mg	Cu	Ni	Cr	Zn	Ti
AA6050	Bal.	1.5	1.55	0.45	0.7	0.325	0.6	0.15	0.25 Max	0.1 Max

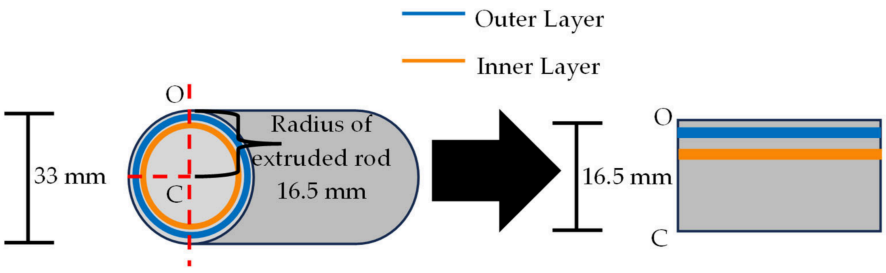


Figure 1. Sections of extruded rod with highlighted regions used for chip collection from machining.

Two regions were selected for the collection of chips, the outer layer and the inner layer, in accordance with industrial practice. Each region had a thickness of 2 mm, as illustrated by the radial sections extending from the centre of the rod (C) to the circumference (O) in Figure 1. Starting from the circumference of the rod, a 1 mm gap towards the centre of the rod was given. The first region of interest is the outer layer with a 2 mm thickness. This

2 mm thickness is associated with the 31–27 mm diameter from the centre of the rod. A further 2 mm gap was then given. The second region of interest is the inner layer with a 2 mm thickness. This 2 mm thickness is associated with the 23–19 mm diameter from the centre of the rod. The chips from the outer and inner layers of the rod were then compared with each other and between alloys for analysis.

After the chips were calculated from the machined sample rods, they were rinsed and dried to remove any cutting fluid residue. The next step was to follow an industrial practice of a chip weight method and count 200 chips, repeated twice more for a total of 600 chips for one layer to obtain an average, and weigh them. Based on this value, the machinability of an alloy at a specific depth of cut can be determined where the number of chips expected for 100 g is calculated. This value is the given machinability for an alloy where the higher it is, the greater the machinability. A total of 7200 chips were assessed via this method using three sample rods for each alloy, which via this method is significantly time-consuming and cumbersome.

The new proposed method is significantly different. This method assessed a total of 28 chips using 1 sample rod for each alloy. Seven rinsed and dried chips from each layer of the extruded rods were collected. They were then placed within a Jeol IT200 SEM where a single image of the fracture face of each chip was taken. A labelled example of a chip is shown in Figure 2. The chip-stock fracture surface (end) is the face of the chip selected for analysis. A clearer image of the identified regions, named SCIL (Shear Crack Initiation Length) and SCPL (Shear Crack Propagation Length), on the chip-stock fracture surface (end) is shown in Figure 3. The SCIL and SCPL are not newly discovered features; their existence is well known. Although they have not been named as SCIL and SCPL, they have been described for both steel [24] and aluminium [25] chips. What is new is the quantification and acronyms (SCIL/SCPL) of these features to the best of the authors' knowledge.

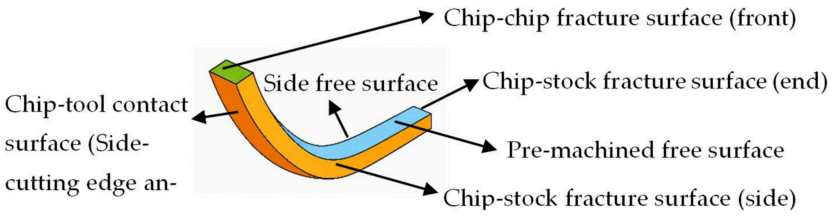


Figure 2. Names given to each side of an example machined chip.

The quantification step required the measurement of the SCIL within the middle third of the chip cross-section at three different points, from which an average SCIL thickness was calculated for each chip. The middle third is approximately indicated by the red circle in Figure 3a with measurement positions that can vary within the middle third but are approximately evenly spaced. The computer software ImageJ (v. 1.54 K) was used, where individual lines were drawn and measured manually. The SCPL region was not used for quantification as in many cases the lower end of this region (Figure 3a) was either damaged, a section was missing, or it protruded outwards due to the way in which the chip detaches from the stock alloy. This made the SCPL vary hugely in thickness and therefore unreliable for analysis.

To evaluate differences in SCIL thickness between the outer and inner layers and between the two alloys, statistical analyses were performed using chip-level averages. Three measurements were taken from each chip and averaged, resulting in seven independent specimen averages for each alloy–layer combination ($n = 7$). Pairwise comparisons were performed using Welch's independent-samples t-tests [26], with Holm correction applied to account for multiple comparisons [27]. The two-way ANOVA was also conducted to identify significant effects of alloy and layer as well as any interaction between these factors [28].

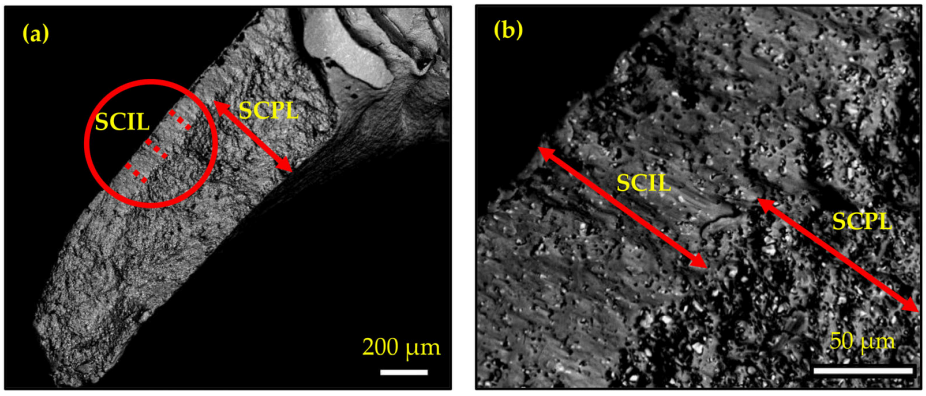


Figure 3. SEM BSE images of an outer layer AA6050 chip from an extruded rod. (**a**) Chip-stock fracture surface with SCIL and SCPL regions, showing highlighted SCIL measurement positions from three dashed red lines. (**b**) Enlarged SCIL region and part of the SCPL region.

3. Results

3.1. Chip Morphology and Size

Figures 4 and 5 show the morphologies of chips formed after machining the inner and outer layers of the extruded rods from AA6050 and the Ca–Sr variant. The outer layer shows chips of two morphologies for both alloys highlighted by the red rectangles. For AA6050 there were 40 long continuous chips formed, whereas the Ca–Sr variant had 73 significantly shorter continuous chips across three rods of each alloy from the outer layer as shown in Figures 4a and 5a. The Ca–Sr variant demonstrates a considerable decrease in the length of these chips compared to AA6050, hence the large increase in the number of shorter continuous chips. The inner layer for both alloys did not form continuous chips. The continuous chips formed in AA6050 are considered more harmful for machinability; therefore, the substantial reduction in size is a significant improvement for machinability with the Ca–Sr variant. The bulk of the chips formed from the outer layer seem to have a similar morphology for both alloys. Figure 5b shows a mixture of half-round chips with a smaller size along with chips seen in Figure 5a. This change in morphology and decrease in chip size of the Ca–Sr variant helps to reduce the weight of each chip, thereby improving machinability as suggested by [20]. Figure 4b shows chips where there are at least one or two curls and some half-round chips, which have contributed to an improvement in machinability due to reduced size and weight compared to Figure 4a.

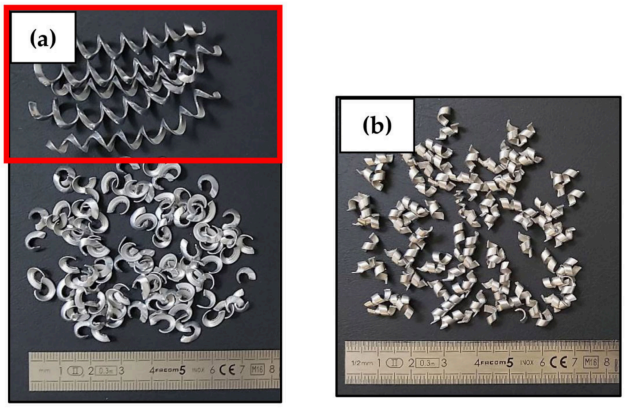


Figure 4. Morphology of chips after machining AA6050 at the outer layer (**a**) and the inner layer (**b**), respectively.

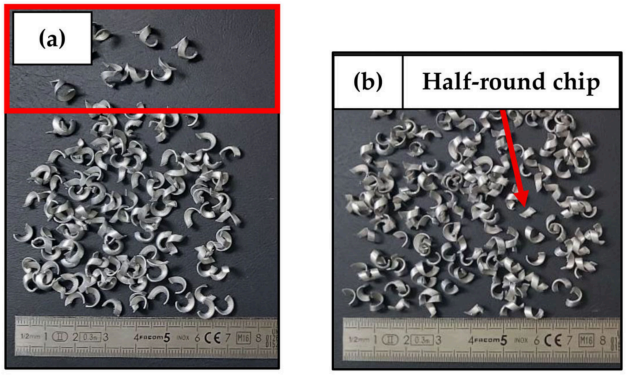


Figure 5. Morphology of chips after machining AA6050 + 0.55 wt.% Ca + 0.27 wt.% Sr at the outer layer (**a**) and the inner layer (**b**), respectively.

3.2. Machinability Assessment According to the Weight Method

Figure 6 shows the average machinability of three rods for both AA6050 and the Ca–Sr variant at the outer and inner layers, the chips of which are shown in Figures 4 and 5. There is a clear improvement with the Ca–Sr variant with respect to both layers, where the value for the No. of Chips/100 g is higher for the Ca–Sr variant. The industrial method shows a trend in machinability, which can be adequate for certain cases. However, the results in Figure 6 seem to show no significant difference in the machinability between layers of the same alloy, which is about 6% for AA6050 from 2540 ± 163 to 2679 ± 60 and 0% for the Ca–Sr variant given that the error bars overlap. There is a difference shown between the same layer of different alloys, which is an improvement for the Ca–Sr variant of about 22% for the inner layer from 2679 ± 60 to 3255 ± 793 and about 28% for the outer layer from 2540 ± 163 to 3248 ± 379. In contrast, Figures 4 and 5 depict a distinct and greater difference in chip morphology and size as explained in Section 3.1. Therefore, chip morphology and size are not well represented by the quantification shown in Figure 6. The large standard deviations of 793 for the inner layer and 379 for the outer layer were attributed to improved and worsened machinability, respectively, observed in one of the three assessed rods compared to the other two rods of the Ca–Sr variant. Figures 4 and 5 qualitatively show a degree of variation in the length and size of chips formed within each layer and alloy, which supports the ambiguous nature of standard machinability assessment and demonstrates the need for a method with more precision for machinability assessment.

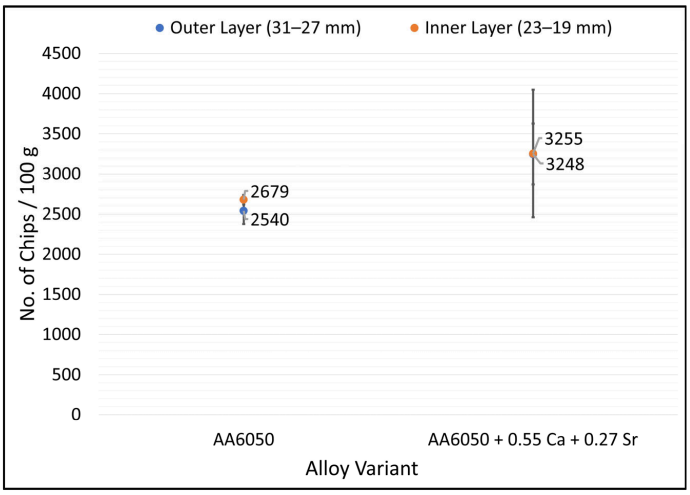


Figure 6. Average machinability of AA6050 and AA6050 + 0.55 wt.% Ca + 0.27 wt.% Sr for all three rods at the outer and inner layers by the weight method with standard deviation.

3.3. Machinability Assessment According to the New Method

By measuring the SCIL shown in Figure 3, the quantified data now correlate more clearly to the morphology and size of the chips. This data shown in Figure 7 demonstrates that the smaller the thickness of the SCIL, the better the machinability of the alloy, which corresponds to smaller/shorter chips as seen in Figures 4 and 5. From the chip images, Figure 4a demonstrates the poorest machinability. An improvement is made with Figure 5a, then Figure 4b, and finally Figure 5b based on the morphology and size of the chips, regardless of whether they are the preferred smaller discontinuous chips or the more harmful long continuous chips. This correlates well with the order of machinability data presented in Figure 7, but not with Figure 6, as both AA6050 and the Ca–Sr variant seem to have the same machinability at both their outer and inner layers.

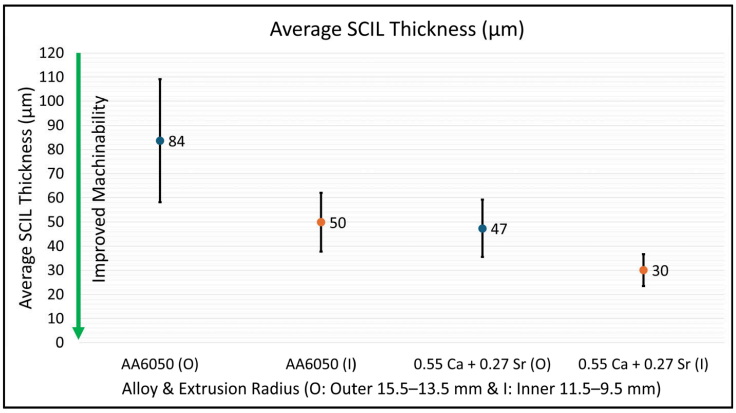


Figure 7. Machinability of extruded alloys AA6050 and AA6050 + 0.55 wt.% Ca + 0.27 wt.% Sr according to thickness of SCIL with standard deviation.

Figure 7 shows a significant difference between the SCIL of the outer and inner layers of AA6050 where an improvement in machinability of about 40% was achieved from 84 ± 25 µm to 50 ± 12 µm. This is deemed an improvement since the reduction in the SCIL correlates with the formation of shorter chips, as seen in the change between Figure 4a (almost forming a full circular loop) and Figure 5a (which resembles a semi-circular morphology). This qualitative reduction in chip size correlates well with the improved machinability shown in Figure 7. The difference between the SCIL layers for the Ca–Sr variant is shown to have achieved an improvement of about 36% from the outer layer to the inner layer, from 47 ± 12 µm to 30 ± 7 µm. At first glance, the morphology of chips from the outer and inner layers of the Ca–Sr variant appears to be almost the same. However, careful inspection by eye shows they are slightly shorter with some significantly shorter forming as half-round chips (Figure 5b). An alloy with more half-round chips forming indicates that the swarf is breaking off the stock more frequently, creating more chips compared to an alloy with relatively continuous chips. The slightly longer chips highlighted in the red rectangle (Figure 5a) of the outer layer are not observed in Figure 5b of the inner layer. These two factors contributed to the improved machinability between layers, which is clear from the correlation between the reduced chip size in Figure 5a, b and the reduction in SCIL shown in Figure 7. The machinability of the inner layer of the Ca–Sr variant has improved significantly compared to the outer layer where the data (Figure 7) and morphology (Figure 5) correspond well with each other. To gain a visual appreciation of the data shown in Figure 7, a comparison of the SCIL from the outer layer of an example AA6050 chip and a Ca–Sr variant chip is illustrated in Figure 8. Statistically, SCIL thickness was significantly greater in the outer layer than in the inner layer for both AA6050 (83.6 ± 25.5 µm vs. 50 ± 12.2 µm, $p = 0.012$) and the Ca + Sr-containing alloy (47.4 ± 11.8 µm vs. 30.1 ± 6.6 µm, $p = 0.008$). Furthermore, AA6050 exhibited significantly greater SCIL

thickness than the Ca–Sr-containing alloy in both the outer layer ($p = 0.008$) and inner layer ($p = 0.004$). All four pairwise comparisons remained statistically significant following Holm correction (adjusted $p \leq 0.023$). Two-way ANOVA revealed significant main effects of alloy ($F(1,24) = 22.52$, $p < 0.001$) and layer ($F(1,24) = 18.62$, $p < 0.001$), whereas the alloy–layer interaction was not statistically significant ($F(1,24) = 1.92$, $p = 0.178$).

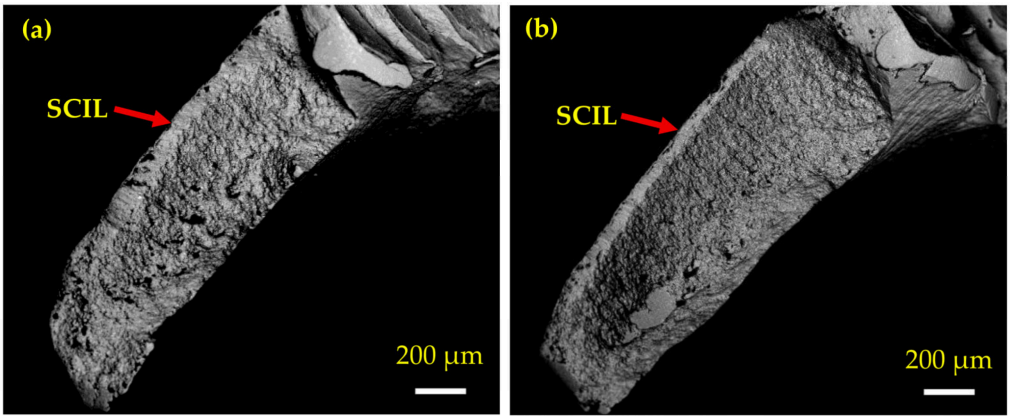


Figure 8. SEM BSE images of the SCIL on the Chip-stock outer layer fracture surface (end view) of (**a**) the AA6050 chip and (**b**) the Ca–Sr variant chip.

4. Discussion

From the literature review in the Introduction, there are a variety of methods which can indicate the machinability of an alloy. Unfortunately, these methods can lack the ability to accurately detect subtle changes in machinability due to alloy chemistry changes, for example. If they do, it could be attributed to a margin of error. Other methods, such as the industrial practice currently used, lack the ability to show an adequate correlation between the calculated machinability and the morphology/size of the chip formed. Therefore, there was a need to create a new method where the morphology/size of the chips formed during machining, correlates more closely with the quantified value of machinability.

Given that machinability is reliant on the point at which a chip breaks off from the alloy (stock), it was thought there may be a feature at the chip-stock fracture surface that can be quantified and measured to determine alloy machinability. Shear failure is the ultimate reason for why a chip breaks off, but the surface at which this failure occurs is not a continuous surface. There are two stages to a chip breaking off. The first is the formation of an immediate shear crack (SCIL), which is then followed by a crack that propagates (SCPL) from this initial shear crack until the chip is broken off from the stock. During aluminium alloy machining, the cutting tool applies high compressive and shear stresses to the material, causing plastic deformation within the primary shear zone. As deformation increases, heat is generated, and thermal softening may cause the strain to concentrate within a narrow region, forming a shear band. Continued deformation allows the shear stress to exceed the material's shear strength; thus, a crack develops which is what the SCIL measures (Figure 3b). Looking at the SCIL feature, it is relatively smooth demonstrating the shear force experienced by the chip. Where the SCIL is shorter in length, this corresponds to greater resistance to shear, which does not permit significant plastic deformation to occur in comparison to relatively longer SCIL thicknesses. The SCPL then forms once more stress is concentrated due to continued loading, which then leads to chip separation due to catastrophic brittle fracture, as demonstrated by the relatively rough surface seen in (Figure 3b).

Based on the formation of the SCIL and SCPL, it was of interest to study the chip-stock fracture surface (end) (Figure 3a) of each layer of the extruded rods to determine if these

features can be quantified. This paper shows that the SCIL can be quantified and correlated to the machinability of an alloy. Figure 9 shows a screenshot from a video recording of an unknown Al alloy, not associated with this paper in any way, which when subjected to machining demonstrates the formation of two shear cracks which are the named SCIL (Figure 9a) and SCPL (Figure 9b). The original video from which Figure 9 was taken belongs to Professor Joseph Datsko and was uploaded with his permission by Raja Kountanya to YouTube.

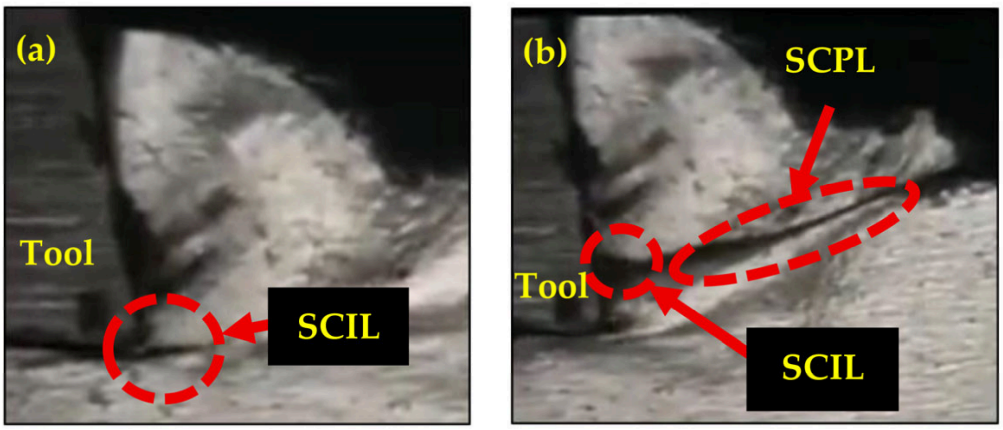


Figure 9. Identification of (**a**) SCIL and (**b**) SCPL from a different unrelated alloy chip during machining. Screenshot reproduced from 'The mechanism of chip formation' [29].

Upon studying the chip-stock fracture surface, the middle third of the chip seemed to remain unaffected by any torsion experienced by the chip, which causes the ends to twist, thereby demonstrating different conditions along the width of chip/tool surface. Looking at either Figure 3a or Figure 8, one can see that both ends of the chips have a different morphology and size due to the torsion experienced at the ends from one side of the chip being free and the other attached to the stock as depicted in Figure 2. It can also be dependent on which side at the point of fracture has a stronger bond causing the weaker side to fail first and initiate the torsion. The middle third experiences little to no torsion and maintains a uniform thickness. It was therefore decided to analyse this region of the chip fracture surface. Across the entire length of the chip there is a noticeable banding separating the chip into two layers as shown in Figure 3. The layer of interest was labelled as the SCIL, since the thickness of this region (identified in Figure 3—AA6050 chip and Figure 9—different unrelated alloy chip) is directly related to the initial shearing that occurs. This region can be quantified and associated with machinability.

The SCIL was notably reduced in thickness for the Ca–Sr-containing alloy variant. Due to the difference in SCIL thickness for different alloys and the improved correlation between the quantified machinability and the morphology/size of the chips, this parameter is proposed as a novel metric to assess the machinability of an alloy with a better correlation to the morphology of the chips formed. A smaller SCIL thickness can be associated with easier chip break-off and a smoother surface finish, offering a more process-relevant alternative to the chip counting and weighing method used by industry.

Given the change in thickness of the SCIL and subsequently the SCPL, it can be assumed that in extreme cases one or the other of the two layers will form the entirety of the chip-stock fracture surface (end). For example, pure Al has the highest ductility compared to Al alloys. Therefore, it would be expected for the SCIL to take most, if not the entire cross-sectional thickness of the chip-stock fracture surface (end). The reason for this suggestion is the correlation between the large SCIL (Figure 7) and the continuous chips formed in the outer layer of AA6050 (Figure 4a). In the reverse case, where the alloy is more brittle it

would be expected for the SCPL to make up most, if not the entire cross-sectional thickness of the chip-stock fracture surface (end). This has been suggested since the correlation between the relatively small SCIL (Figure 7) and the appearance of shorter chips with some being half-round in morphology have been observed in the inner layer of the Ca–Sr variant (Figure 5b). Therefore, small half-round chips, which are preferred over the continuous chip form, should have a minimal/non-existent SCIL thickness. Half-round chips are deemed better with respect to machinability due to their small size and the excellent surface finish they provide, as given by the Aluminium Association's rating system for machinability in order of decreasing merit from A to E [30], where A is given the description of "free cutting, very small broken chips and excellent surface finish."

In theory, the SCIL and SCPL, be it one or a combination of both, can form in all Al alloys and any other alloy subjected to machining. If confirmed with more experiments across a range of alloys not only limited to Al based alloys, this new method can pave the way to possibly being used as a universal and efficient technique to find the machinability of an alloy. This will remove the ambiguity of current methods where they can provide an indication or a trend but lack the precision to differentiate between sample layers and similar alloys. This level of precision will give both industry and academia improved data driven decisions regarding the machinability of their alloys.

Further research is required regarding this new technique to assess machinability. This includes testing with a variety of Al alloys and other alloys such as steels. Given the observations regarding the formation of the SCIL and SCPL, it can be expected for these features to form in every chip. Further optimisation of the technique is possible by reducing the number of assessed chips from seven to three or four, which will significantly reduce the assessment turnaround time. Instead of taking approximately half a working day to assess 28 chips, it could be reduced to 14 chips taking only a few hours from the point of collecting chips from the lathe to obtaining the SCIL thickness. This is an achievable step, which will result in a substantial time saving, thereby improving productivity. Either number of chips assessed using this new technique is still significantly faster than the current industry weight-based method, which can take two working days from collecting the chips to obtaining a machinability value in this experimental case.

5. Conclusions

The focus of this study was to find and develop an alternative method to those currently available, which can be used as a sole machinability indicator, improving the correlation between chip morphology/size and the quantified machinability result. The main conclusions are:

(1) A new process-relevant method has been developed that quantifies the layer named SCIL to be used as a sole indicator for machinability, assuming machining input parameters and the depth of cut for identically shaped, processed, and treated samples are the same for comparison against another alloy.
(2) The new method has improved the correlation between the quantified results and the physical change in morphology/size of the chips created during machining.
(3) The new method provides users with greater clarity when differentiating between the machining performance of different alloys, especially those that have been subjected to minor compositional changes in chemistry.
(4) The new method gives a significant improvement in assessment turnaround time compared to the current industrial practice, from about two working days to half a working day with the potential to be reduced further to a few hours, which improves productivity.
(5) Future studies can investigate the relationship between SCIL thickness and other important aspects of machining performance, such as cutting forces, tool wear, surface

roughness, cutting temperature, and chip disposal, to determine the robustness of SCIL thickness being used as a sole indicator of machinability.

Author Contributions: Conceptualization, A.R.A.; Formal analysis, A.R.A.; Funding acquisition, D.G.E. and C.B.; Investigation, A.R.A.; Methodology, A.R.A.; Project administration, N.S.B.; Resources, D.G.E. and N.S.B.; Supervision, D.G.E. and C.B.; Validation, A.R.A.; Writing—Original Draft, A.R.A.; Writing—Review & Editing, A.R.A., D.G.E. and N.S.B. All authors have read and agreed to the published version of the manuscript.

Funding: The authors gratefully acknowledge the financial support of the UK Engineering and Physical Sciences Research Council (EPSRC Grant: Industrial CASE Account—Brunel University 2020, under grant number EP/V519480/1, project reference 2625304) and Constellium, Ltd.

Data Availability Statement: The raw/processed data required to reproduce these findings cannot be shared at this time due to legal reasons and forms part of an ongoing study.

Acknowledgments: The authors thank Ivan Skalicky for the pilot-scale billet castings from which the extruded rods were subsequently produced, John Guntrip for the machining of the extruded rods from which the swarf was collected, Chandra Bhanu Basak for providing the drawing in Figure 2, and the Experimental Techniques Centre (ETC) at Brunel University of London for the use of their Jeol IT200 SEM.

Conflicts of Interest: The authors declare no conflicts of interest.

Abbreviations

The following abbreviations are used in this manuscript:

Al	Aluminium
PRT	Platinum Resistance Thermometers
SCIL	Shear Crack Initiation Length
SCPL	Shear Crack Propagation Length
SEM	Scanning Electron Microscope

References

1. Vargel, C. *Corrosion of Aluminium*; Elsevier Science: Oxford, UK, 2004. [CrossRef]
2. Stephenson, D.A.; Agapiou, J.S. *Metal Cutting Theory and Practice*, 3rd ed.; CRC Press: Boca Raton, FL, USA, 2016. [CrossRef]
3. Trent, E.M.; Wright, P.K. *Metal Cutting*, 4th ed.; Butterworth-Heinemann: Boston, MA, USA, 2000. [CrossRef]
4. *ISO 3685:1993*; Tool-Life Testing with Single-Point Turning Tools, 2nd ed. ISO: Geneva, Switzerland, 1993.
5. *ISO 8688-1:1989*; Tool Life Testing in Milling—Part 1: Face Milling. ISO: Geneva, Switzerland, 1989.
6. Taylor, F.W. On the Art of Cutting Metals. *Trans. ASME* **1906**, *28*, 31–279. [CrossRef]
7. Childs, T.; Maekawa, K.; Obikawa, T.; Yamane, Y. *Metal Machining: Theory and Applications*; Butterworth-Heinemann: Oxford, UK, 2000.
8. Gonçalves, R.A.; da Silva, M.B. Influence of Copper Content on 6351 Aluminum Alloy Machinability. *Procedia Manuf.* **2015**, *1*, 683–695. [CrossRef]
9. Attia, M.H.; Kops, L. Distortion in Thermal Field around Inserted Thermocouples in Experimental Interfacial Studies. *J. Eng. Ind.* **1986**, *108*, 241–246. [CrossRef]
10. Attia, M.H.; Kops, L. Distortion in Thermal Field around Inserted Thermocouples in Experimental Interfacial Studies—Part II: Effect of the Heat Flow through the Thermocouple. *J. Eng. Ind.* **1988**, *110*, 7–14. [CrossRef]
11. Attia, M.H.; Kops, L. Distortion in the Thermal Field around Inserted Thermocouples in Experimental Interfacial Studies—Part 3: Experimental and Numerical Verification. *J. Eng. Ind.* **1993**, *115*, 444–449. [CrossRef]
12. Attia, M.H.; Cameron, A.; Kops, L. Distortion in the Thermal Field around Inserted Thermocouples in Experimental Interfacial Studies, Part 4: End Effect. *J. Manuf. Sci. Eng.* **2002**, *124*, 135–145. [CrossRef]
13. Stephenson, D.A. Tool-Work Thermocouple Temperature Measurements—Theory and Implementation Issues. *J. Eng. Ind.* **1993**, *115*, 432–437. [CrossRef]
14. Martinovský, M.; Mádl, J. The Effect of Different Modifiers on Cutting Temperature in Turning of AlSi7Mg0.3 Alloy. *Manuf. Technol.* **2018**, *18*, 950–953. [CrossRef]

15. Industrial Administration and Engineering Production Group Applied Mechanics Group; Boothroyd, G. Temperatures in Orthogonal Metal Cutting. *Proc. Inst. Mech. Eng.* **1963**, *177*, 789–810. [CrossRef]
16. Yoshioka, H.; Hashizume, H.; Shinno, H. In-Process Microsensor for Ultraprecision Machining. *IEE Proc. Sci. Meas. Technol.* **2004**, *151*, 121–125. [CrossRef]
17. Davies, M.A.; Ueda, T.; M'Saoubi, R.; Mullany, B.; Cooke, A.L. On the Measurement of Temperature in Material Removal Processes. *CIRP Ann.* **2007**, *56*, 581–604. [CrossRef]
18. Balogun, V.A.; Mativenga, P.T. Impact of Un-Deformed Chip Thickness on Specific Energy in Mechanical Machining Processes. *J. Clean. Prod.* **2014**, *69*, 260–268. [CrossRef]
19. Liao, Z.; Schoop, J.M.; Saelzer, J.; Bergmann, B.; Priarone, P.C.; Splettstößer, A.; Bedekar, V.M.; Zanger, F.; Kaynak, Y. Review of Current Best-Practices in Machinability Evaluation and Understanding for Improving Machining Performance. *CIRP J. Manuf. Sci. Technol.* **2024**, *50*, 151–184. [CrossRef]
20. Du, H.; Karasev, A.; Stavlid, N.; Björk, T.; Lövquist, S.; Jönsson, P. Using Chip Weight Distribution as a Method to Define Chip Breakability during Machining. *Procedia Manuf.* **2018**, *25*, 309–315. [CrossRef]
21. Barekar, N.S.; Skalicky, I.; Barbatti, C.; Fan, Z.; Jarrett, M. Enhancement of Chip Breakability of Aluminium Alloys by Controlling the Solidification during Direct Chill Casting. *J. Alloys Compd.* **2021**, *862*, 158008. [CrossRef]
22. Mills, B.; Redford, A.H. *Machinability of Engineering Materials*; Applied Science Publishers: London, UK, 1983. [CrossRef]
23. The Aluminum Association, Inc. *International Alloy Designations and Chemical Composition Limits for Wrought Aluminum and Wrought Aluminum Alloys*; The Aluminum Association, Inc.: Arlington, VA, USA, 2025. Available online: https://www.aluminum.org/sites/default/files/2026-01/Teal%20Sheets%20December%202025.pdf (accessed on 24 May 2026).
24. Elbestawi, M.A.; Srivastava, A.K.; El-Wardany, T.I. A Model for Chip Formation during Machining of Hardened Steel. *CIRP Ann.* **1996**, *45*, 71–76. [CrossRef]
25. Lin, J.T.; Bhattacharyya, D.; Ferguson, W.G. Chip Formation in the Machining of SiC-Particle-Reinforced Aluminium-Matrix Composites. *Compos. Sci. Technol.* **1998**, *58*, 285–291. [CrossRef]
26. Welch, B.L. The Generalization of 'Student's' Problem when Several Different Population Varlances are Involved. *Biometrika* **1947**, *34*, 28–35. [CrossRef] [PubMed]
27. Holm, S. A Simple Sequentially Rejective Multiple Test Procedure. *Scand. J. Stat.* **1979**, *6*, 65–70. Available online: https://www.jstor.org/stable/4615733 (accessed on 3 November 2026).
28. Nesselroade, K.P., Jr.; Grimm, L.G. (Eds.) Two-Way Analysis of Variance. In *Statistical Applications for the Behavioral and Social Sciences*, 2nd ed.; Wiley: Hoboken, NJ, USA, 2018; pp. 425–482. [CrossRef]
29. Kountanya, R. The Mechanism of Chip Formation. YouTube. 2015. Available online: https://www.youtube.com/watch?v=2fDJ1Wky04 (accessed on 15 January 2025).
30. Spillard, C.M. Alloy 6020: A Lead-Free Aluminum Alloy Featuring "A" Rated Machinability. In *SAE Technical Paper Series*; Technical Paper 980459; SAE International: Warrendale, PA, USA, 1998. [CrossRef]

Disclaimer/Publisher's Note: The statements, opinions and data contained in all publications are solely those of the individual author(s) and contributor(s) and not of MDPI and/or the editor(s). MDPI and/or the editor(s) disclaim responsibility for any injury to people or property resulting from any ideas, methods, instructions or products referred to in the content.